OPEN ACCESS

University of BRISTOL

Scott, S., Capuzzi, M., Langston, D., Bossanyi, E., McCann, G., Weaver, P. M., & Pirrera, A. (2017). Effects of aeroelastic tailoring on performance characteristics of wind turbine systems. *Renewable Energy*, *114*(B), 887-903. https://doi.org/10.1016/j.renene.2017.06.048

Publisher's PDF, also known as Version of record

License (if available):
CC BY

Link to published version (if available):
10.1016/j.renene.2017.06.048

Link to publication record in Explore Bristol Research
PDF-document

University of Bristol - Explore Bristol Research

General rights

This document is made available in accordance with publisher policies. Please cite only the published version using the reference above. Full terms of use are available:
http://www.bristol.ac.uk/pure/about/ebr-terms

Renewable Energy 114 (2017) 887–903

Contents lists available at ScienceDirect

Renewable Energy

journal homepage: www.elsevier.com/locate/renene

Effects of aeroelastic tailoring on performance characteristics of wind turbine systems

Samuel Scott [a], Marco Capuzzi [a], David Langston [a], Ervin Bossanyi [b], Graeme McCann [b], Paul M. Weaver [a], Alberto Pirrera [a, *]

[a] Bristol Composites Institute (ACCIS), Department of Aerospace Engineering, University of Bristol, Queen's Building, University Walk, Bristol, BS8 1TR, UK
[b] DNV GL, One Linear Park, Avon Street, Bristol, BS2 0PS, UK

ARTICLE INFO

Article history:
Received 7 March 2016
Received in revised form
10 May 2017
Accepted 12 June 2017
Available online 18 June 2017

Keywords:
Aeroelastic tailoring
Variable stiffness
Wind turbine blade
Load alleviation
Composites
Bend-twist coupling

ABSTRACT

Some interesting challenges arise from the drive to build larger, more durable wind turbine rotors. The rationale is that, with current designs, the power generated is theoretically proportional to the square of the blade length, however, theoretical mass increases cubically. Aeroelastic tailoring aims to improve the ratio between increased power capture and mass by offering enhanced combined energy capture and system durability. As such, the design and full system analysis of two adaptive, aeroelastically tailored wind turbine blades is considered herein. One makes use of material bend-twist coupling, whilst the other combines both material and geometric bend-twist coupling. Each structural design meets a predefined coupling distribution, that approximately matches the stiffness of a baseline blade.

The performance characteristics of the wind turbine systems are assessed and compared in terms of power production, load alleviation and pitch system considerations. The blade with both couplings displays scope for potential increases in energy yield. Additionally, beneficial flapwise load alleviation is demonstrated by the adaptive blades from both International Electrotechnical Commission prescribed fatigue, and extreme operational gust analysis. Finally, the adaptive blades display power smoothing capabilities and reductions in pitch rate, however, increases in blade root torsional moment possibly contrast these pitch system benefits.

© 2017 The Authors. Published by Elsevier Ltd. This is an open access article under the CC BY license (http://creativecommons.org/licenses/by/4.0/).

1. Background

There is a trend in the wind turbine industry towards larger rotor diameters, due to their capacity for greater energy capture. This trend is part of a drive to reduce the overall cost of wind energy. However, larger rotors increase aerodynamic and inertial loading which, in turn, places a greater structural demand on key components such as blades, drivetrain and tower. To avoid bigger loads increasing the cost of energy (CoE), it is desirable to employ load alleviation strategies. The obvious benefits of load alleviation are: (i) extending the lifetime of components, particularly those whose designs are fatigue driven; (ii) reducing the amount of structural material for weight and cost savings; (iii) enabling larger rotors for increases in annual energy yield (AEY) for new and retrofitted turbines.

Conventional load management strategies of wind turbines (WTs) employs active pitch control of the full blade using actuators at the blade root. However, alternative ways of achieving load control in a passive manner allow blades to vary their aerodynamic characteristics, hence their performance, in response to changing environmental conditions. Various ways of achieving a tailored adaptive response have been proposed, including deformation coupling and morphing aerodynamic devices, where much inspiration has been gained from research on aircraft wings and helicopter blades [1,2]. Swept aircraft wings, for example, have an inherent geometric coupling between bending and twisting deformations which can lead to undesirable resonant interactions. Previous work has shown that such instabilities can be kept within allowable limits by embedding anisotropy in the wing structure to induce material bend-twist coupling (BTC) [3].

In the field of WTs, aeroelastic tailoring makes use of BTC to induce twisting of the blade in response to flapwise bending. For example, an increase in wind speed (i.e. a gust) causes a downwind bending deformation. In a tailored blade, this deformation induces a nose-down twist (towards feather) such that the blade's angle of attack decreases thus reducing loads. This behaviour gives the

* Corresponding author.
E-mail address: alberto.pirrera@bristol.ac.uk (A. Pirrera).

http://dx.doi.org/10.1016/j.renene.2017.06.048
0960-1481/© 2017 The Authors. Published by Elsevier Ltd. This is an open access article under the CC BY license (http://creativecommons.org/licenses/by/4.0/).

Nomenclature

β^*	pitch angle at $C_{p_{max}}$
$\dot{\beta}$	pitch rate
ω	rotational speed
σ	standard deviation of power
τ	pitch actuator torque
θ	ply angle
C_p	power coefficient
F	weibull distributed probability
K_{opt}	constant of proportionality
M	bending moment
T	total simulation time
t	simulation time
V	wind speed
ADC	actuator duty cycle
AEY	annual energy yield
BTC	bend-twist coupling
CA	combined adaptive
CoE	cost of energy
DEL	damage equivalent load
DLC	design load case
EOG	extreme operating gust
GA	genetic algorithm
IEC	international electrotechnical commission
IPC	individual pitch control
LE	leading edge
MA	material adaptive
MW	megawatt
NREL	national renewable energy laboratory
TE	trailing edge
TSR	tip-speed ratio
WT	wind turbine

blade an inherent load alleviation capability, or passive load control. Initial studies in this field examined a nose-up twist response for promoting stall, however, such a response is only relevant for stall-regulated turbines and more increases fatigue loading [4].

This paper focuses on aeroelastic tailoring that induces a nose-down twist response, as this promotes load alleviation in variable-speed, pitch regulated WTs.

2. Introduction

There are different ways of incorporating BTC into a wind turbine blade that fall into two broad categories: geometric and material coupling. Geometric coupling is induced by a curved, or swept, blade planform; whereas material coupling is induced by anisotropic composite materials. Generally, for material coupling, off-axis plies are used to unbalance the composite laminates. However, Hayat et al. [5] also explore other means such as using multiple materials and variable ply thicknesses to create an unbalance. Additionally, Herath et al. [6] propose an alternative design that displays BTC, using spanwise stiffeners that vary their stiffness in the chordwise direction.

As regards geometric coupling, Ashwill [7] presents the results from a project carried out by Knight and Carver, in which a Sweep Twist Adaptive Rotor blade is designed, built and tested. The rotor diameter is increased from 48 m to 54 m, giving a measured power output increase of 12% with no increase in flapwise loads. Similarly, the use of swept blades is now in commercial use by Siemens [8], where an existing blade is modified to have sweep and extended in length from 49 m to 53 m. This, along with other technological advances, allows increases in AEY and little change in load levels. Larwood et al. [9] present a parametric study of three swept blade designs with varied power ratings. Gains in AEY of 5% are achieved with increased rotor diameter, but the swept 5 MW blade suffers a twist instability at high wind speeds, confirming that stability is an important consideration when aeroelastically tailoring larger blades. This finding is also supported by Lobitz et al. [10], where flutter speed is shown to reduce for an aeroelastically tailored blade.

Botasso et al. [11] present a multi-disciplinary optimisation tool for the structural design of WT blades with material BTC. Blades with various off-axis fibre angles are designed and analysed. Additionally, blades with coupling starting at different outboard locations are compared, with the preferred solution starting the off-axis plies from 30% span outwards, to maintain load alleviation capabilities whilst saving weight. A similar design is offered by Larwood et al. [9], in which sweep is preferred only in the outboard portion of the blade to reduce manufacturing complexity. Botasso et al. find benefits such as reductions in damage equivalent loads (DEL), minimal losses in power and a positive synergistic effect between individual pitch control (IPC) and the passive capabilities. Gözcü et al. [12] consider a material-coupled structural design of the NREL 5 MW [13] blade that maintains similar stiffnesses to the baseline model. The authors used Samcef Wind Turbines, a Siemens analysis software, to perform fatigue analyses and compare DELs in the blade root and gearbox, where reductions in fatigue loads are found in the coupled designs. A key limitation of this study is the single wind speed (15 ms^{-1}) considered, whereas a more thorough fatigue analysis could have been made by analysing the WT over its whole operating range - as specified by the International Electrotechnical Commission (IEC) standards.

The combination of both material and geometric coupling has been proposed by Capuzzi et al. [14–16], where the blade's steady twist deformation at rated is precisely tailored using spatially variable BTC to meet a pre-defined distribution. The prescribed twist distribution is output from an optimisation study, with the objective of maximising energy capture. Specifically, starting from the root, the magnitude of the output nose-down twist angle increases towards the mid-span then decreases towards the tip. This twist curve contrasts with previous work, where only *either* material *or* geometric coupling is used and the magnitude of twist increases monotonically with blade radius. These distributions are displayed in Fig. 1, where a negative angle indicates the nose-down direction. In order to compare the aeroelastic performance of tailored blades featuring monotonic and non-monotonic twist deformations, two design configurations are considered in this work: one with material coupling and one with material and geometric coupling. The two adaptive configurations are henceforth referred to as the 'combined-adaptive' (CA) design, due to the use of two couplings, and the 'material-adaptive' (MA) design. Aeroelastically, a design with solely geometric coupling would behave similarly to the MA design. This third case is therefore not taken into consideration. Load alleviation, from IEC gust analysis, and increases in steady AEY of at least 1%, are displayed by Capuzzi et al.'s CA design.

The aim of the current work is to provide a thorough comparison between the MA and CA blade designs, in terms of power performance, load alleviation and pitch system considerations. Two

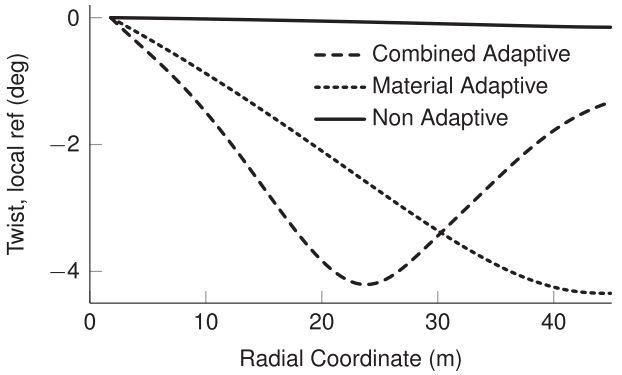

Fig. 1. Figure illustrating 'non-adaptive', 'material-adaptive' and 'combined-adaptive' twist responses - Reproduced from Ref. [17].

WTs are used for comparison: the NREL 5 MW [13], and a 7 MW model provided by DNV GL. The NREL 5 MW is used as it is a recognisable, research-standard WT. However, it is based on technology that is now over a decade old and there is some uncertainty in blade properties such as shear centre and reference axis orientations, these being important for aeroelastic analyses of BTC blades [18]. Due to it being relatively old, it is no longer that representative of current/future technology (for example, it has a less advanced design of aerodynamic profile and control algorithms, as demonstrated by the fact that the pre-twist optimisation of the baseline yielded an increase in AEY of 1.02%). Therefore, the 7 MW model has also been used as it is an optimised design, offering a realistic representation of current commercial technology and well-defined blade properties. Key properties of both WTs are displayed in Table 1. It is noted that both WTs use the same set of aerofoils. For each WT, MA, CA and baseline designs are considered, giving a total of six WTs for comparison.

The paper is organised as follows. Firstly, a study is made into the optimal elastic twist response with respect to power, then the adaptive designs for each coupling configuration are proposed, including structural detail and steady torque control considerations. Results from an IEC prescribed gust analysis are then discussed, as this load case induces the greatest coupling response and thus clearly highlights the maximum potential of the adaptive behaviour. Next, a set of realistic dynamic simulations, conforming to IEC standards [19], are used to assess the effects of tailoring on the whole system behaviour. From this data, comparisons are made on power production, fatigue loads and pitch system effects. Lastly, a flutter stability analysis is presented to check flutter safety margins in the large, coupled blades. Note, DNV GL's Bladed is used for all steady and dynamic aeroelastic analyses. The aerodynamic model is based on blade element momentum theory [20] with Prandtl's tip and hub loss corrections [21]. Additionally, dynamic wake and dynamic stall models are based on the works of Pitt and Peters, and Beddoes-Leishman/Øye, respectively [22–24]. The structural model is based on a multi-body dynamics approach [25] with a modal representation of flexible components. All other subsystems, including power train, nacelle, tower and control algorithms are represented by relevant models with full details found in Ref. [26].

3. Twist optimisation study

Similarly to the approach taken by Capuzzi et al. [14], the first step in designing the CA blade is a twist optimisation study that maximises blade energy capture through aeroelastic tailoring. Only key results and comparisons relevant to this study are presented here. For a full description of the design process the reader is referred to [14].

Table 1
Blade properties.

Parameter	NREL 5 MW [13]	DNV GL 7 MW (in-house data)
Rotor orientation/ configuration	Upwind, three blades	Upwind, three blades
Control	Variable speed, collective pitch	Variable speed, individual pitch
Rated power (MW)	5	7
Blade Length (m)	61.5	77.7
Cut in, rated, cut out wind speed (ms^{-1})	3, 11.4, 25	3, 11, 25
Cut in, rated rotor speed (rpm)	6.9, 12.1	3.98, 10.74

The initial results from the twist optimisation are shown in Fig. 2a, where only those for the 7 MW WT are depicted as they are feature-wise the same as those for the NREL 5 MW. For comparison purposes, the results from Ref. [14] are also shown in Fig. 2b. Each line in these figures represents the optimal *total* twist angle of a single spanwise blade station and shows the ideal variation between cut-in and rated with respect to maximising power. Here, *total* twist is measured relative to the rotor plane and is the sum of *static pre-twist*, *dynamic twist deflection* and *pitch angle* (note that, in contrast to Capuzzi et al. [14,15], in the below-rated operating region the pitch angle is fixed at 0 deg, as 'fine pitching' is not considered herein).

Fig. 2a shows that all radial stations maintain a relatively constant twist angle between cut-in and rated, which is to be expected from a variable-speed WT for which the blade geometry is optimised. The torque controller keeps the blade in an optimal operating condition, maintaining a constant tip-speed ratio (TSR) and thus maximum power coefficient (C_p). Therefore, if any variations in blade twist could possibly yield more power, one could conclude that there is some sub-optimality in either the blade design or the control law. This sub-optimality is displayed in Fig. 2b where a nose-up twist towards the middle of the operating range then nose-down twist towards rated is shown to be optimal for maximising power. Hence, the torsionally rigid baseline blade causes a significant loss in power compared to this optimal solution. However, Capuzzi et al. show that by designing spatially varying BTC into the blade this power loss can be mostly recovered - making a significant power improvement on the baseline.

It is proposed that the source of the previously discussed sub-optimality found in Ref. [14] arises from the control law that is input to the twist optimisation, this being input in terms of rotational speed as a function of wind speed $\omega(V_0)$. For reference purposes, the sub-optimal curve is indicated by the dash-dot line in Fig. 3, where $\omega(V_0)$ is plotted and non-dimensionalised by the rated wind speed and rated rotational speed, on the x and y axis, respectively. This allows the curves to be feature-wise readily comparable. The sub-optimal curve reaches rated rotational speed well before rated wind speed, possibly due to noise constraints or cost considerations limiting the maximum generator speed. However, there is often a trade-off in such multi-disciplinary designs and as the WT used in Ref. [14] is in commercial production, it can be assumed that this choice of control law was a justified decision in terms of overall cost.

For comparison purposes, Fig. 3 also displays the optimal curve used by the 7 MW WT, which is indicated by the solid black line and shows that the rotational speed increases proportionally with wind speed throughout most of the whole below-rated range, so as to

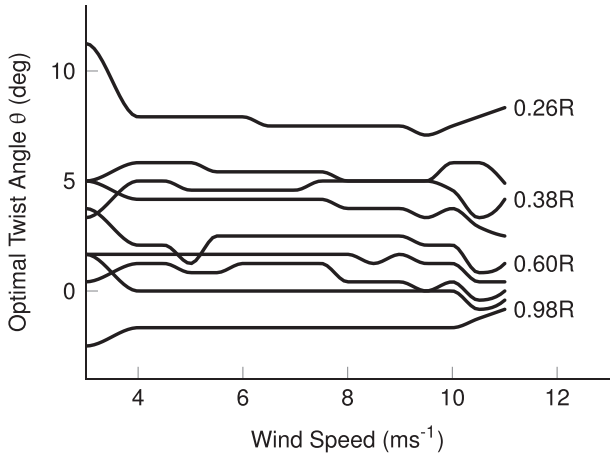

(a) DNV GL 7 MW blade.

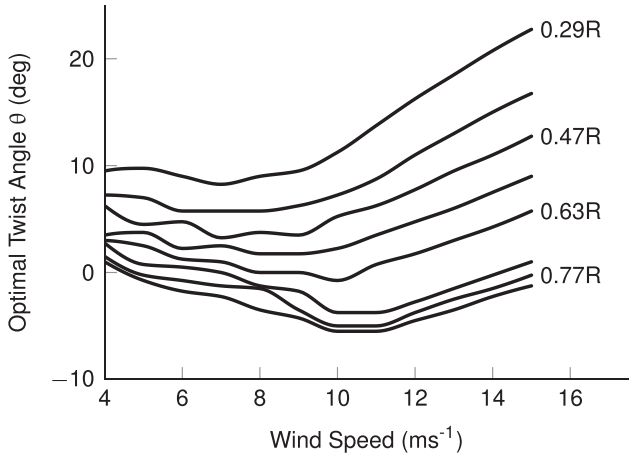

(b) Reproduced from [14].

Fig. 2. Optimal twist curves for each blade radial station, with respect to maximising power.

maintain a constant TSR and C_p. It is noted that the optimal curve still reaches rated rotational speed before rated wind speed, thus displaying a small sub-optimality and offering the potential for power gains, however, whether this could be exploited is unclear from the twist curves. Additionally, a turbulent curve for this WT is shown by the dashed lined, further indicating the differences between the optimal and sub-optimal distributions and also how, when considering turbulent results, rated wind speed is not actually fixed and depends on the turbulence intensity.

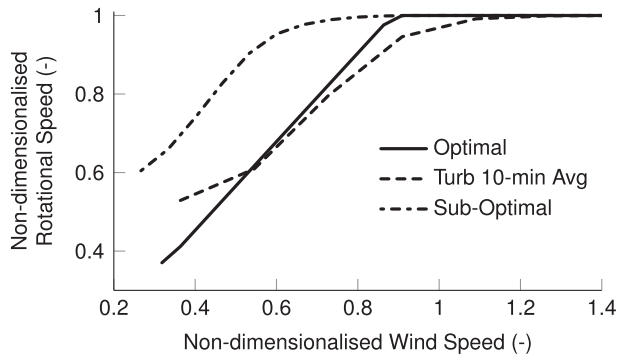

Fig. 3. Comparison of non-dimensionalised rotational speed curves.

A key result from this section is that, if a WT follows the optimal $\omega(V_0)$ curve, aeroelastic tailoring does not offer substantial gains in AEY. This leaves load alleviation as the remaining attribute to be exploited by such tailoring. However, MA solutions with monotonic elastic twist response are generally associated with small decreases in AEY, where the more significant the coupling, the more significant the power loss [11]. As energy capture is a significant contributor to CoE, it is desirable to avoid any losses. Therefore, in proposing MA and CA designs, this work aims to investigate how aeroelastic tailoring can influence the relationship between energy capture and load alleviation, and to find out if load alleviation is possible whilst minimising, or even negating, a loss in AEY. Whilst this comparison study is made for blades with fixed rotor radius, it is noted that reductions in flapwise loading can still improve AEY, and thus reduce CoE, by allowing for increases in blade length. However, the impact of increasing blade length on CoE requires the complex consideration of the WT system as a whole and is not considered here.

4. Adaptive blade design

In this section, the structural design for adaptive blades is detailed. Furthermore, with the introduction of elastic twist deflections, static-twist distributions of a blade are considered to be non-optimal and thus are optimised with respect to maximising AEY. Finally, some insight is given into the steady control procedure below rated and how it could be improved.

4.1. Structural design

Our primary aim is to provide a structural design of an aeroelastically tailored blade that displays a specific MA or CA twist deflection at rated loading, as this is where the turbine spends most time operating. A secondary objective is that the blade should maintain mass and stiffness distributions similar to those of the baseline, to ensure that the resulting adaptive design are feasible and comparable. These aims are similar to the inverse design process used by Gözcü et al. [12]. As stated in the previous section, the motivation for designing the CA blade is that of load alleviation whilst minimising any losses in AEY. However, with no exact twist response from the optimisation study, it is chosen to only follow the shape of the twist response seen in Refs. [14,15], as it still provides the inherent load alleviation of a nose-down response but with less influence on the tip section of the blade. There is no numerical justification for the exact magnitude of twist response chosen, only to maximise the difference between the mid-span twist and the tip twist. The design of the MA twist response is then driven by the desire for straightforward comparison between the adaptive blades, thus the magnitude of tip twist is chosen to match the mid-span twist of the CA blade.

In this design process, spanwise blade properties are first computed using PreComp (Pre-processor for Computing Composite Blade Properties [27]), a software that integrates a modified classical laminate theory with a shear flow approach. PreComp requires inputs at each chosen radial station, such as the blade's external and internal geometry, material properties and lay-up definitions for each laminate section. The spanwise properties from PreComp are then input into DNV GL's Bladed, and a steady aeroelastic analysis is run to compute the twist deflection at rated wind speed. Bladed models flexible components, including blades, with a modal approach, where the total deformation is a linear combination of mode shapes. The mode shapes are calculated using linear finite

element analysis with three-dimensional beam elements to define the mass and stiffness properties. BLADED requires the full WT definition, including all aerodynamic, structural, mechanical and electrical information.

The external geometry of the blade is pre-defined by existing data. For the internal geometry, no data is available, thus a conventional configuration is chosen incorporating a single spar box, made up of spar caps and shear webs. Skin sections provide the aerodynamic shape for the leading edge (LE) and trailing edge (TE). The spar caps are made of monolithic composite materials, whilst the shear webs and skins are sandwich panel constructions to avoid buckling. This internal geometry is displayed in Fig. 4. Additionally, the root and tip sections are made entirely of monolithic composite materials. Specifically E-Glass/Epoxy and a medium-density foam are used, with properties shown in Table 2. The lay-up definitions for each section are shown in Table 3, where θ indicates the off-axis plies and, for the sandwich panels, 'F' indicates the foam core. For simplicity, lay-up definitions and thicknesses are identical between top and bottom spar caps, fore and aft shear webs, and LE and TE sandwich panels. Better designs would have more detailed variations between panels, however, this would require local stress analysis which is unavailable with PRECOMP. Laminate thicknesses for each design are displayed in Figs. 5 and 6.

To introduce BTC into the MA blade, off-axis plies of constant angle are located in both the spar cap and skins. Similarly to Botasso et al. off-axis plies are used only in the outer 70% of the blade span to target maximum aeroelastic benefits while minimising potential weight gain. Blade masses are displayed in Table 4. It is noted that, in this case, there is a mass increase because off-axis plies cause a decrease in global bending stiffness compared to 0 deg fibres. Here we use off-axis fibre angles of 9 deg and 7 deg for the NREL 5 MW and DNV GL 7 MW, respectively, which were found by trial-and-error to best meet the desired magnitude of tip twist, whilst approximately meeting baseline stiffness and mass distributions. For the CA blade, a combination of geometric and material coupling is used, as done by Capuzzi et al. [15,16]. Rearward sweep is used to induce a global nose-down coupling, whilst off-axis plies of variable angle are used to vary the amount of coupling locally. Off-axis plies are placed in both the skin and spar caps, and span the whole length of the blade. These features are displayed in Figs. 7 and 8. For both designs, off-axis plies make up between 60 and 85% of the laminate thicknesses, with generally higher proportions in the spar caps. Small percentages of 90 deg and ± 45 deg fibres are included to account for secondary loading. The resulting twist responses, at the WTs' steady-rated wind speeds, are shown in Fig. 9.

It is noted that specifying the number of blade modes to be used in the aeroelastic calculations is important for capturing accurate torsional dynamics and, in turn, accurate loads and power. However, a larger number of modes incur greater computation times, therefore a compromise is made with 11 blade modes for all simulations. Additionally, appropriate blade mesh density is important for correct modal representation, therefore, the 7 MW blade model uses 32 stations as provided by DNV GL, where this has been tested for mesh convergence using fatigue loads as the convergence criteria. The NREL 5 MW uses 19 stations as this is the

Table 2
Material properties [28].

Material	E-Glass/Epoxy	Foam (F)
E_{11} (GPa)	39.0	0.1
E_{22} (GPa)	8.6	0.1
G_{12} (GPa)	3.8	0.1
ν_{12} (−)	0.28	0.3
ρ (kgm^{-3})	2100.0	100.0

Table 3
Lay-up definitions.

Location	Lay-up
Spar Cap	[θ 45 0 -45 90 90 -45 0 45 θ]
Skin Sandwich	[θ/45/0/-45/90/F/90/-45/0/45/θ]
Shear Web Sandwich	[45/-45/F/-45/45]

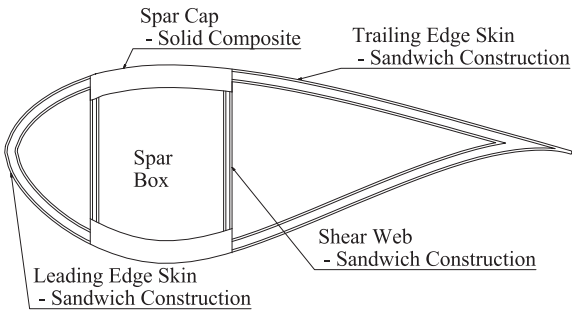

Fig. 4. Sectional internal geometry - not to scale.

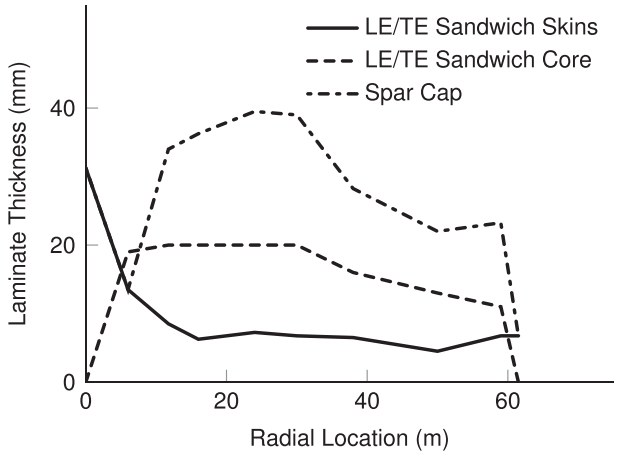

(a) Material-adaptive.

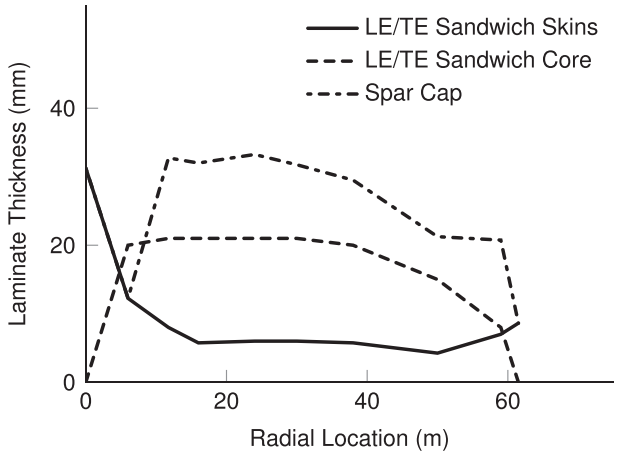

(b) Combined-adaptive.

Fig. 5. Laminate thicknesses along the blade length - NREL 5 MW.

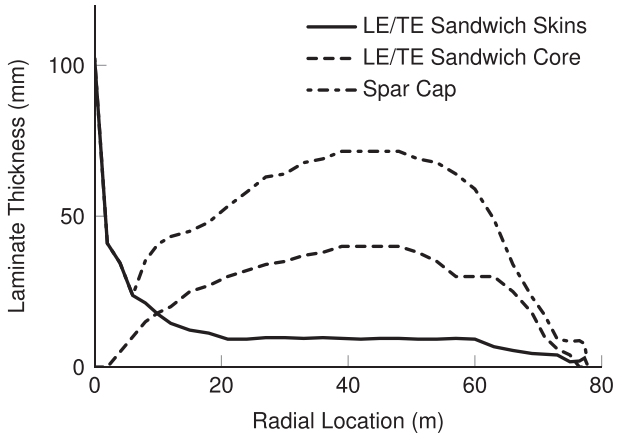

(a) Material-adaptive.

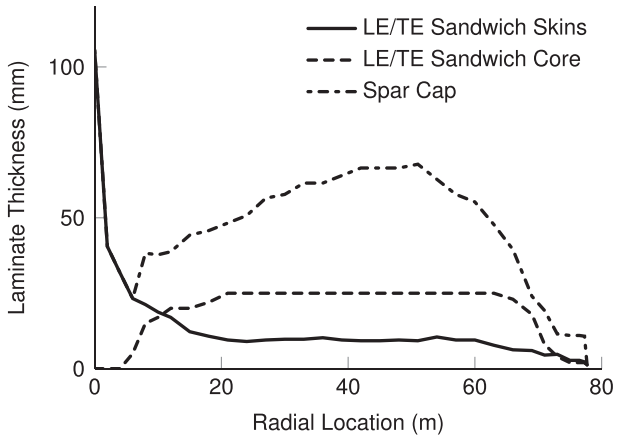

(b) Combined-adaptive.

Fig. 6. Laminate thicknesses along the blade length - DNV GL 7 MW.

maximum resolution from the aerodynamic data provided in Ref. [13].

As an initial assessment of the effect of tailoring upon the blade modal interactions, the first five blade modal frequencies are displayed in Table 5. It can be seen that tailoring reduces all blade modal frequencies due to coupling, marginal changes in stiffness and changes in mass. For both WTs, the first blade mode is safely above the range of operating frequencies (0.115–0.202 Hz for the NREL blade and 0.066–0.179 Hz for the 7 MW blade). However, whilst blade modal frequencies may provide some information

Table 4
Total blade masses and percentage differences to the baseline.

(a) NREL 5 MW		
	Blade Mass	Difference (%)
B	16762	–
MA	17138	2.24
CA	16344	−2.49
(b) DNV GL 7 MW		
	Blade Mass	Difference (%)
B	34725	–
MA	37929	9.23
CA	37282	7.36

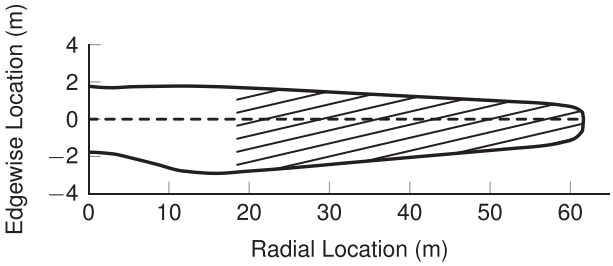

(a) Material-adaptive.

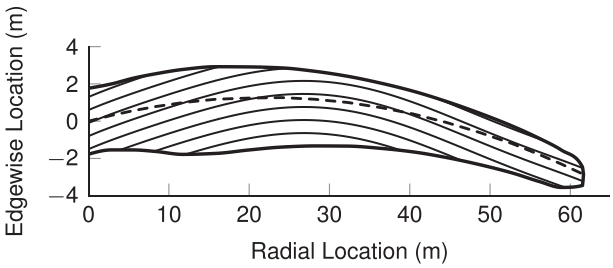

(b) Combined-adaptive.

Fig. 7. NREL 5 MW - Fibre orientation and sweep curvature.

regarding modal interactions, more information can be gained from a Campbell Diagram, in which combined rotor and tower modes are calculated and plotted on a frequency diagram. Combined modes are made up from a combination of relevant blade/tower/drivetrain modes and provide a more accurate representation of the likely deformation patterns of the overall structure. Such diagrams are not shown here for reasons of brevity. However, they confirm that aeroelastic tailoring does not induce resonant interactions with 1P

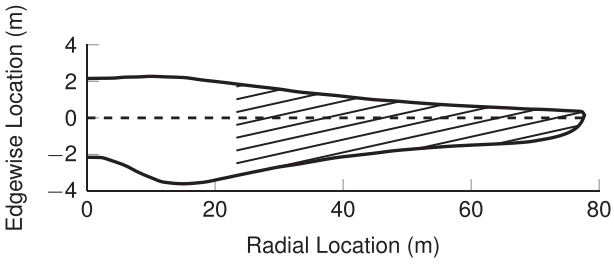

(a) Material-adaptive.

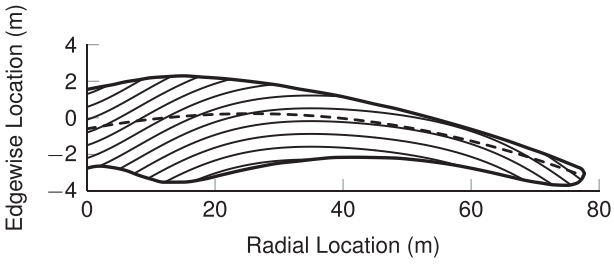

(b) Combined-adaptive.

Fig. 8. DNV GL 7 MW - Fibre orientation and sweep curvature.

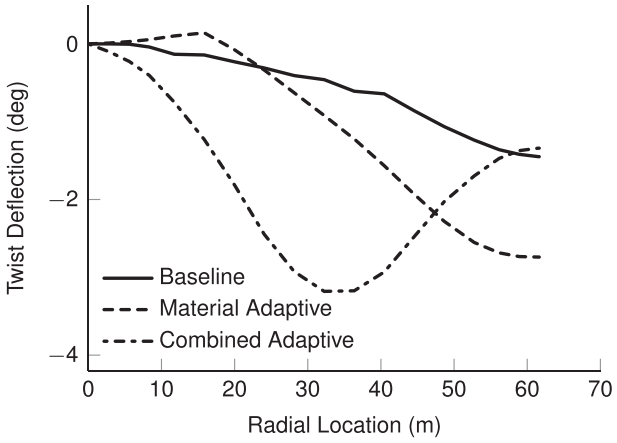

(a) NREL 5 MW

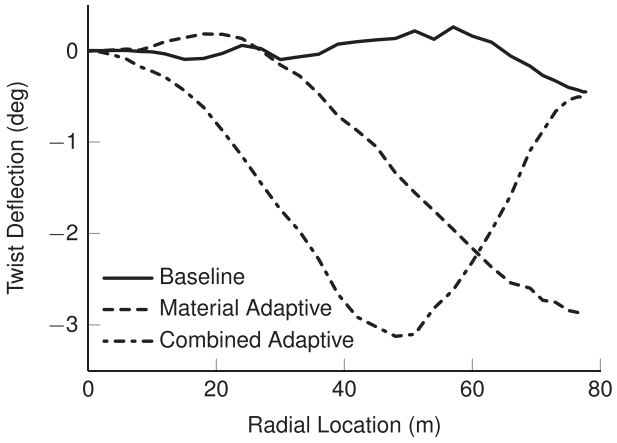

(b) DNV GL 7 MW

Fig. 9. Steady twist deflections at rated wind speed.

or 3P harmonics.

It is noted that the proposed designs are not optimal. Weight savings could be made with an improved design, potentially including carbon fibre sections in the spar caps. Spar box geometry could also be optimised as described in Ref. [29]. Additionally, it is noted that concerns have been raised regarding the accuracy of PreComp especially when anisotropic materials are included [30]. However, as this work only aims to provide a top-level structural design, with more emphasis on the results of the aeroelastic studies, blade designs that display the intended coupling behaviour are assumed to be structurally feasible as already shown in Ref. [16].

4.2. Static-twist optimisation

With the introduction of significant elastic twist deflections in the adaptive blades, it can be assumed that using the baseline blade static-twist distribution is sub-optimal for power production. In Ref. [14], Capuzzi et al. approach this problem by setting the twist such that

$$\text{static-twist} = \text{ideal total twist (at rated)} - \text{elastic twist (at rated)}, \quad (1)$$

where the ideal total twist is an output from the initial twist optimisation study. This solution offers a 'rated-optimised' design, however, it is also observed that a 'rated-optimised' design results in slightly lower AEY than an 'AEY-optimised' design. Hence, explaining why AEY is generally the output to be maximised in the design of the blade aerodynamic profile. In contrast, Stäblein et al. set static-twist so that the angle of attack distribution at a design wind speed matches that of the baseline [31].

Table 5
Blade modal frequencies up to the first torsional mode. F = flapwise, E = edgewise, T = torsional.

(a) NREL 5 MW

Blade Mode	Modal Frequency (Hz)		
	B	MA	CA
1	0.751 F	0.625 F	0.600 F
2	1.083 E	1.048 E	1.051 E
3	2.109 F	1.872 F	1.840 F
4	4.060 E	3.740 E	3.786 E
5	4.812 F	4.282 F	4.172 F
6	5.792 T	6.093 T	5.790 T

(b) DNVGL 7MW

Blade Mode	Modal Frequency (Hz)		
	B	MA	CA
1	0.527 F	0.473 F	0.456 F
2	0.842 E	0.793 E	0.783 E
3	1.505 F	1.418 F	1.364 F
4	2.677 E	2.528 E	2.461 E
5	3.096 F	2.953 F	2.860 F
6	5.110 F	4.812 F	4.626 F
7	5.860 E	5.360 T	5.495 T
8	6.209 T	5.742 E	5.650 E

In this work a single-objective optimisation study is made to find blade twist distributions that maximise AEY. Blade twist distribution is considered as the decision variable and is encoded using a three point Bezier curve for the NREL 5 MW and a five point spline for the DNV GL 7 MW. This difference allows the optimiser to find a solution with detail similar to that provided by the baseline model, where for the 7 MW blade a sharp increase in twist at the tip aids with tip losses and noise. Bladed is used as the model for this optimisation, where a steady aeroelastic calculation is run between cut-in and rated wind speed, a power curve is output and AEY calculated from this. It is noted that for all AEY calculations in our work, a Weibull distribution of wind speeds is used with mean wind speed of 8.5 ms^{-1}, shape factor 2 and availability 85%. As the design space is found to be non-convex, a Genetic Algorithm (GA) is used within Matlab as the optimiser. A globally optimal solution is ensured by choosing large values for population size (50) and number of generations (10). Other parameters such as crossover and mutation functions are left as default by the Matlab GA function. Baseline blade static-twist distributions are also optimised for consistency.

The final static-twist curves are displayed in Fig. 10, where it is noted that the differences between the optimal baseline curve and each adaptive curve are similar to the respective adaptive twist deflections at least in shape rather than magnitude. This result indicates that for each WT there is an 'AEY-optimised' twist distribution where the optimiser finds a static-twist curve that, roughly summed with the twist deflection, equals this optimal twist curve. This finding is similar to that presented by Capuzzi et al. and seen in Equation (1), albeit with differences in magnitude and a dependency on the wind distribution used. However, this similarity is less apparent for the static-twist values closer to the root, as this section has less influence on the aerodynamic forces generated and thus minimal influence on the optimisation.

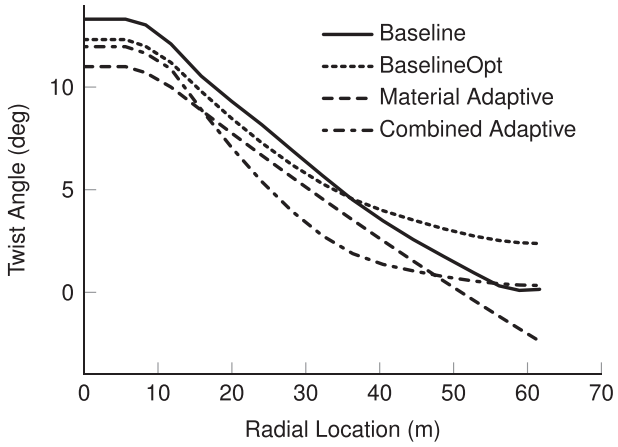

(a) NREL 5 MW

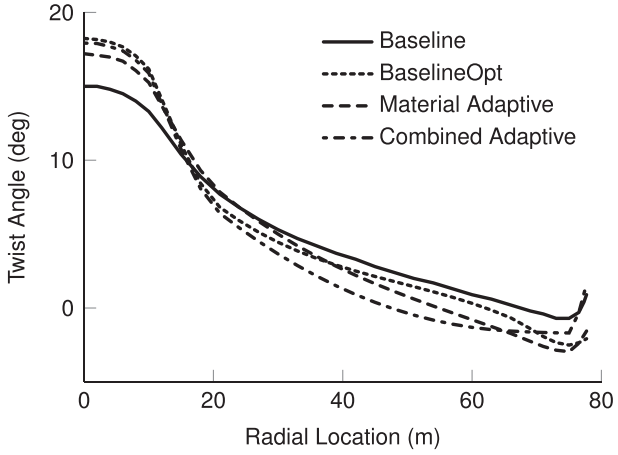

(b) DNV GL 7 MW

Fig. 10. Optimal twist distributions.

The increases in AEY for each blade are shown in Tables 6 and 7. For both baseline blades there is an increase in AEY from the static-twist optimisation, however, this is far more significant for the NREL blade. It is possible that the NREL blade is designed from a purely aerodynamic point of view, and thus does not consider the fact that the baseline has a reasonable elastic twist deflection at rated, as shown in Fig. 9a. Consequently, this optimisation finds significant AEY gains as it considers aeroelastic effects and thus structural twist deflections. A similar optimisation has been carried out in Ref. [32], albeit only for rigid blades. Here, we find that with an increased number of points used to specify a twist distribution, greater increases in AEY can be obtained, due to an increased 'waviness' of the optimal twist curve that is facilitated by the greater design freedom. Indeed, the optimised 7 MW design

Table 6
AEY results from static-twist optimisation - NREL 5 MW.

Blade	AEY (MWh)	AEY Optimised (MWh)	Difference (%)
B	17056	17164	0.64
MA	17041	17145	0.61
CA	17009	17188	1.05

Table 7
AEY results from static-twist optimisation - DNV GL 7 MW.

Blade	AEY (MWh)	AEY Optimised (MWh)	Difference (%)
B	25265	25300	0.14
MA	24761	25234	1.91
CA	24798	25394	2.41

improves on its baseline AEY using such freedom. It is also noted that whilst Botasso et al. [11] do not vary the blade static-twist, they do vary the blade trim pitch settings which is thought to achieve a similar function as the optimisation made here.

The blades with optimised static-twist are taken forward for all further studies detailed in this work.

4.3. Control law modification

Both WTs considered in this work are variable speed, hence the control strategy below rated is via torque control. For a given blade profile, there is a a single pitch angle (β^*) and TSR that maximises C_p. Therefore, with the aim of maximising power in below rated schemes, the controller keeps the rotating blade as close to the optimal pitch angle (β^*) and TSR as possible. This is done by varying the demanded torque from the rotor such that the rotor speed varies linearly with wind speed and keeps the TSR constant. For steady aeroelastic calculations, this control law is specified as a torque-speed curve, where the demanded generator torque is proportional to the generator speed squared. Here the constant of proportionality is K_{opt}.

As the tailored blades are no longer torsionally rigid, it may not be appropriate to assume that there is a single $C_{p_{\max}}$ that remains constant throughout the operating range. From cut-in to rated the blade twist can change by about 3 deg, therefore the $C_{p_{\max}}$ and corresponding TSR may actually vary in this range. In turn, it is thought that with respect to optimising power, there may be a preferable steady torque-speed curve for the adaptive blades rather than the standard squarely proportional curve.

Here, an optimisation is used to find a series of K_{opt} values for the range of wind speeds between cut-in and rated. At each wind speed, the optimiser finds the K_{opt} value that corresponds with maximum power. The generator speed and demanded generator torque are recorded at each point and a new torque-speed curve is generated. These new curves are displayed in Fig. 11 along with the baseline curves. It is noted that the NREL 5 MW curve has transition regions included either side of the ideal region, whereas the 7 MW follows the ideal curve from its minimum to its maximum generator speed. It can be seen that the new torque-speed curves for the adaptive blades deviate from the ideal curves. Additionally, the optimiser was run for the baseline blades, with no deviation from the ideal curves observed. Small changes in steady AEY from this optimisation are displayed in Tables 8 and 9. As yet, it is uncertain what effects this might have when used in turbulent simulations, however, the effects of shape adaptivity may be of significance when designing adaptive torque controllers to react to time-varying wind, as done by Diaz-Guerra et al. [33].

Here, shape adaptiveness in the steady control law below rated has been considered, however, expanding on this for the dynamic controller was considered outside the scope of this work. Therefore, these control law modifications are not taken forward for the aeroelastic analyses presented in the following sections, but could form the basis for interesting future work.

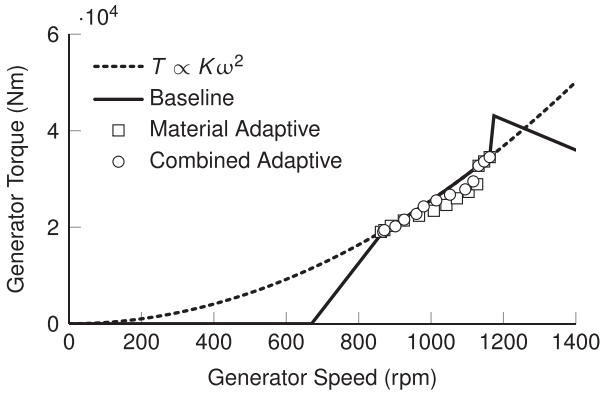

(a) NREL 5 MW

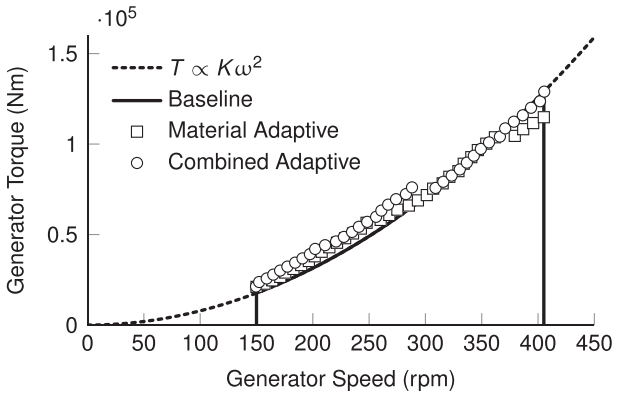

(b) DNV GL 7 MW

Fig. 11. Modified torque-speed curves.

5. Aeroelastic analyses and results

5.1. Gust analysis

The performance of the two adaptive configurations is now compared through a gust analysis. Due to the extreme nature of a gust scenario, the observed responses are highly dependent on the blade's adaptive behaviour, which being elastic develops almost instantaneously. The dynamic control algorithms which, in this case are not re-tuned for the adaptive blades, are also not sufficiently fast to respond to gust and therefore have minimal influence. In contrast, the elastic BTC can be thought of as a kind of inherent structural control law that mitigates loads. A gust load induces a large coupling response that reacts faster than the pitch system can, thus showing the effectiveness of the adaptive behaviour's potential independently of the controllers. Furthermore, maximum loads from gust analyses are often design driving, thus if reductions are observed then this firmly indicates the potential for beneficial design changes, such as removal of material.

Dynamic simulations of the WT systems are run with an extreme operating gust (EOG) input as specified by the IEC design requirements [19]. A single gust case was chosen to display representative results, however, the authors can confirm that a full design load case (DLC) 2.3 analysis was also undertaken to ensure that results displayed here are consistent with the turbine response in all extreme cases. The wind speed distribution used for the 7 MW WT is shown in Fig. 12, where V_{hub} is equal to steady-rated wind speed plus 0.5 ms^{-1} to ensure the initial operating state is at rated and not slightly below. This wind speed gives the highest loads and thus the greatest effect from the adaptive behaviour. Here, only results for the DNV GL 7 MW are shown as similar behaviour is observed for both WTs. It is noted that exponential wind shear of exponent 0.2, tower shadow effects with a combined potential flow/empirical model and flow inclination of 8 deg are included, as is typical for an onshore site.

The electrical power signal during the EOG is displayed in Fig. 13a, where it can be seen that both adaptive designs reduce the power lost in the overshoot, with the CA performing slightly better. Fig. 13b displays the variation in rotational speed through the EOG, where peak values and amplitude of oscillation reduce for the adaptive designs. Both results are promising for power output, in terms of power quality to the grid and also reducing the risks of overspeed situations that could result in a shut down. Additionally, the smoothing of rotational speed could reduce the peak stresses in the drivetrain and generator.

Fig. 14a displays the blade root flapwise bending moment where peak values and amplitude of oscillation are shown to reduce for the adaptive blades. A further reflection of this load alleviation is shown in the tower root nodding moment, displayed in Fig. 14b, where these results reflect changes in the mass, and thus dynamics, of the whole rotor/nacelle assembly. Again, both adaptive designs show reductions in peak values and amplitude of oscillation with the CA performing slightly better. Percentage reductions in peak loads and oscillatory amplitudes are given in Table 10.

Fig. 15a shows the pitch angle response during the EOG simulation. Reductions in peak values are seen for both adaptive designs with a slightly greater smoothing effect for the CA design. Additionally, a slight delay is shown for the adaptive designs indicating that the passive response is alleviating some of the load

Table 8
Control modified AEY comparisons - NREL 5 MW.

Blade	AEY (MWh)	AEY Control Mod (MWh)	Difference (%)
MA	17169	17173	0.02
CA	17261	17263	0.008

Table 9
Control modified AEY comparisons - DNV GL 7 MW.

Blade	AEY (MWh)	AEY Control Mod (MWh)	Difference (%)
MA	25234	25240	0.02
CA	25394	25404	0.04

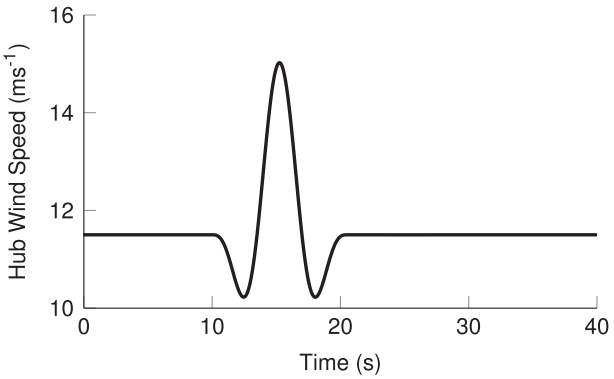

Fig. 12. Gust wind speed profile.

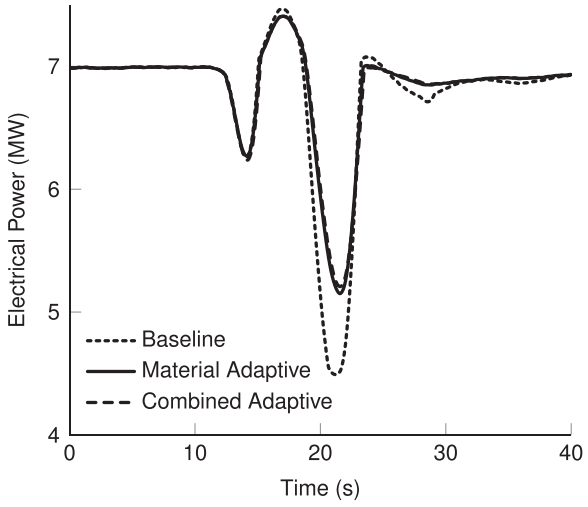

(a) Electrical Power.

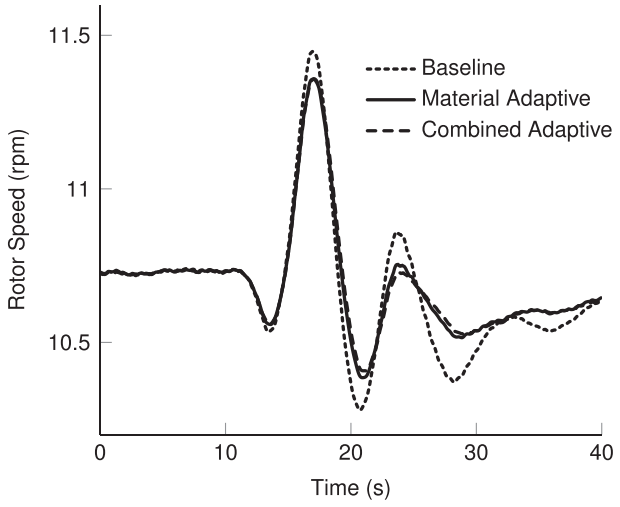

(b) Rotational Speed.

Fig. 13. Output results from EOG simulation.

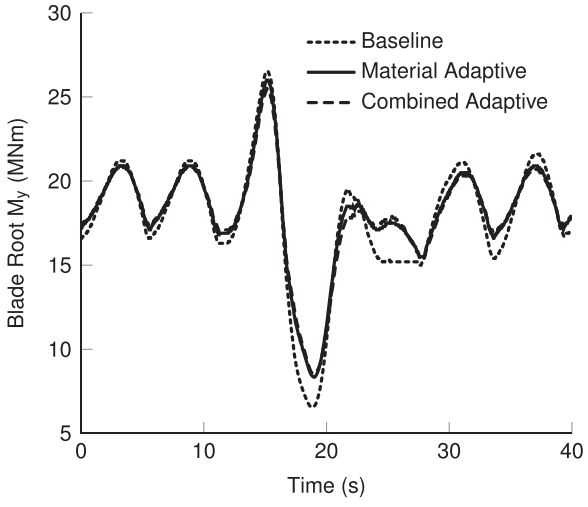

(a) Blade root flapwise moment M_y.

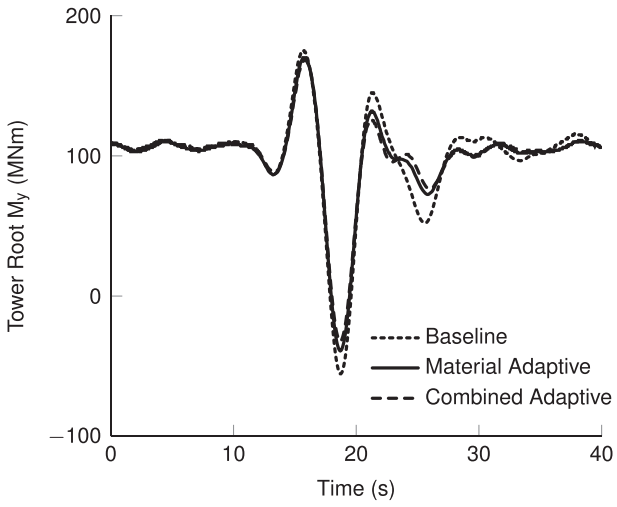

(b) Tower root nodding moment M_y.

Fig. 14. Output results from EOG simulation.

immediately such that the pitch controller receives the input, and thus reacts, slightly later. This delay is confirmed by the reductions in peak pitch rate, as displayed in Fig. 15b. Both of these results display benefits for the pitch system in terms of magnitude and speed of response, which could lead to reductions in wear on various pitch system components.

Overall, the CA design performs marginally better than the MA design in terms of power smoothing, load alleviation and pitch system effects. However, to investigate this result more thoroughly, distributions of blade loading are compared at the point of maximum flapwise loading ($t = 15.2$ s). The distributed aerodynamic loading on the blade at this time is displayed in Fig. 16a where the mid-portion of the CA blade is shown to be more alleviating than the tip. Additionally, the crossover point at 60 m span where one becomes more load alleviating than the other, corresponds exactly with the crossover point in twist deflections shown in Fig. 9b; directly illustrating the fact that greater nose-down twist deflections result in greater load alleviation. However, it is the distribution of this load alleviation that influences the changes in the blade internal shear force (Fig. 16b) and thus the overall blade/tower root bending moments. For example, the MA blade was chosen to have off-axis plies in the outer 70% of the blade span to save weight. However, if tailoring started at the root, whilst meeting the same tip twist deflection, then the crossover point as mentioned above would move further inboard and the blade would, overall, alleviate more flapwise load. This example illustrates how simply matching mid-span and tip twist deflections, as done here, does not result in a completely fair comparison of load alleviation. Therefore, it is not possible to generally state that either coupling configuration, material or combined, is more load

Table 10
Percentage reductions in gust peak and oscillatory loads for the DNV GL 7 MW, relative to the baseline.

Load	Location	MA (%)	CA (%)
Peak M_y	Blade Root	−1.95	−4.30
	Tower Root	−2.76	−3.98
Oscillatory M_y	Blade Root	−12.03	−15.69
(max-min)	Tower Root	−9.12	−12.95

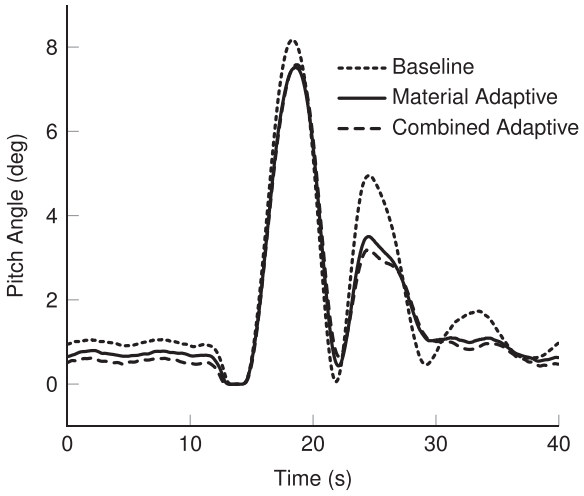

(a) Pitch angle.

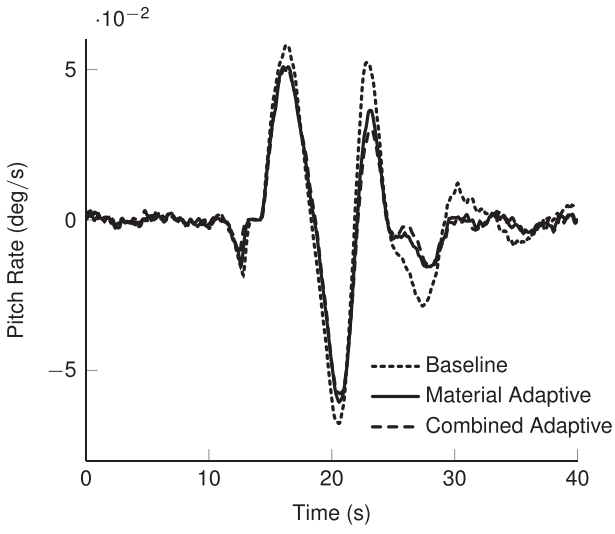

(b) Pitch rate.

Fig. 15. Output results from EOG simulation.

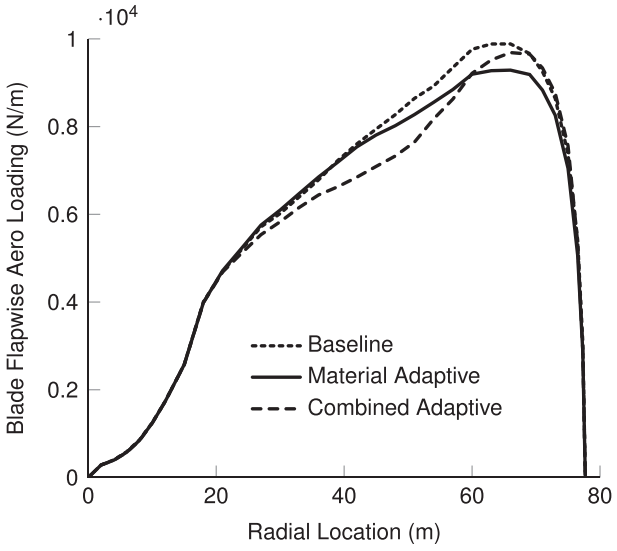

(a) Blade flapwise aerodynamic loading.

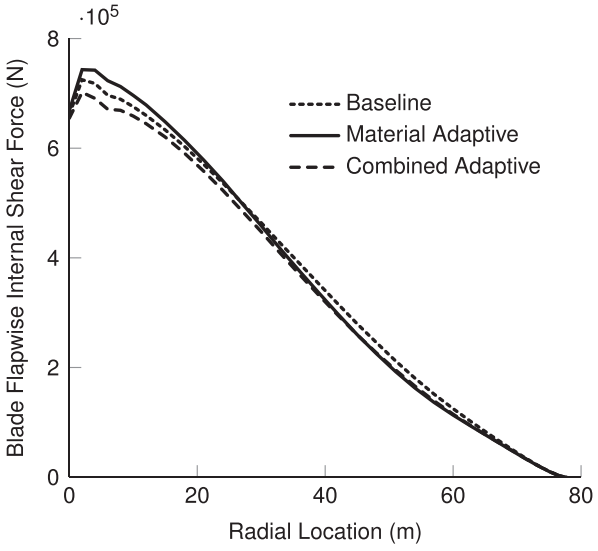

(b) Blade flapwise internal shear force.

Fig. 16. Blade spanwise loads from the gust simulation at $t = 15.2$ s.

alleviating than the other; because factors such as the distribution of coupling and the blade aerodynamic profile influence the location and magnitude of the loads alleviated.

5.2. Analysis and results from turbulent simulations

In this subsection, a series of dynamic simulations provide overall comparison parameters. The full WT system is modelled with all aero-servo-elastic interactions accounted for, including the external dynamic controllers provided for each WT. It is noted that controllers have not been re-tuned for the adaptive blades as this modification lies outside the scope of current work. Additionally, whilst the NREL blade is specified as having collective pitch control, individual pitch control is used for both blades to provide a clearer comparison.

Power production simulations are run according to design load case (DLC) 1.2, as specified in the IEC design requirements [19]. These simulations span the range of wind speeds between cut-in and cut-out, with intervals of 2 ms^{-1}. Additionally, idling simulations are run according to DLC 6.4 for wind speeds below cut-in and above cut-out. It is noted that these simulations provide a simplified load set, appropriate for the comparison analyses used in this work. For each mean wind speed, six 10-minute simulations are run with randomly generated turbulence seed such that any irregularities in wind speed can be averaged out. The turbulence is as specified by IEC [19], using the Kaimal turbulence model assuming WT class II and turbulence intensity B. Similarly to the gust analysis, other features of the simulations include: exponential wind shear of exponent 0.2, tower shadow effects with a combined potential flow/empirical model and flow inclination of 8 deg.

5.2.1. Power production analysis

A comparison of the power production characteristics for each adaptive design is now provided. Comparisons are made from steady aeroelastic calculations and time-averaged power production simulations (DLC 1.2).

Both steady and turbulent power curves are displayed in Fig. 17 for each WT. Only curves for the baseline blades are displayed, as there are no clearly discernible differences between them and those for the adaptive blades. Each point on the turbulent curve is a time-average of the electrical power for the six simulations at that mean wind speed, therefore smoothing of the turbulent curves around rated is noted. This smoothing happens because, for a given turbulent simulation near rated, the wind speed oscillates above and below rated. Electrical power follows these oscillations below rated, however, for rated speed and higher it is capped at rated power, thus reducing the calculated average for that simulation. This smoothing results in a higher 'turbulent-rated' wind speed than the 'steady-rated' value, with a dependency on the level of turbulence.

Clearer comparisons in power output are observed from AEY values, shown in Tables 11 and 12. For the steady results, both MA designs offer a decrease in power as presented in previous studies [11,34]. In contrast, both CA designs offer an increase in steady AEY. A possible explanation here is that the CA twist deflection allows the blade to better match the optimal twist curves displayed in Fig. 2a. Whilst the curves are relatively flat compared to those shown in Fig. 2b, there remains a slight pitch toward feather at the end of the range which may be better matched by the CA twist deflection and so allow for the slight increase in steady AEY observed here. As this feature of the optimal twist curves is relatively minor, the associated gains in AEY are relatively minor compared to those shown in Ref. [15]. However, there remain differences of 0.25% (NREL 5 MW) and 0.63% (DNV GL 7 MW) in AEY between the MA and CA designs indicating the potential superiority in power production.

The turbulent AEY results display a seeming lack of consistent trends, however, the underlying simulations are far more complex than the steady analyses, with many inter-dependent factors at work. Both adaptive NREL blades show an increase in AEY compared to the baseline, with the MA yielding slightly greater power, whilst both adaptive 7 MW blades show decreases, with the CA decrease being more significant and the MA showing near-negligible difference. It is noted that for turbulent simulations, the full WT dynamics are considered using an external dynamic controller that, at least for the 7 MW WT, is tuned specifically for the baseline blade. The dynamic pitch controller is designed to damp out collective modes with low damping, however, introducing sweep into the adaptive blade varies the modal characteristics quite significantly. This effect could leave the controller less able to damp out collective modes that have been modified by tailoring, an effect that is likely to be more significant for the CA blade and could be responsible for the observed decreases in AEY. Furthermore, it is assumed that the NREL controller is of a simpler design and less specific to particular blade dynamics. If the NREL controller is less dependent on the blade dynamics, then it may prove more robust for differing adaptive designs and allow benefits to be observed.

This discrepancy in results, if attributable to the reasons given, highlights the importance of proper controller design for adaptive blades and also how aeroelastic tailoring can affect the dynamics of the system as a whole. For a more consistent comparison it would have been more appropriate to re-tune the controllers for the adaptive blades, or alternatively, fully redesign the dynamic controllers to work in synergy with the adaptive behaviour [11]. However, as already stated, such design of dynamic control systems was considered outside the scope of this work.

As shown in the Gust Analysis section, the distribution of BTC defines which adaptive design is more load alleviating. Similarly, this distribution also affects the power characteristics, and whilst it is clear that the CA design has the potential for greater AEY, from steady results, there may be an optimised coupling distribution that performs better. Equally for the MA design, variations in the coupling may produce greater load alleviation but also a greater

Table 11
Steady and Turbulent AEY comparisons - NREL 5 MW.

(a) Steady.		
	Steady AEY (MWh)	Difference (%)
B	17164	–
MA	17145	−0.11
CA	17188	0.14
(b) Turbulent.		
	Turbulent AEY (MWh)	Difference (%)
B	16589	–
MA	16685	0.58
CA	16651	0.37

Table 12
Steady and Turbulent AEY comparisons - DNV GL 7 MW.

(a) Steady.		
	Steady AEY (MWh)	Difference (%)
B	25300	–
MA	25234	−0.26
CA	25394	0.37
(b) Turbulent.		
	Turbulent AEY (MWh)	Difference (%)
B	23524	–
MA	23519	−0.02
CA	23407	−0.49

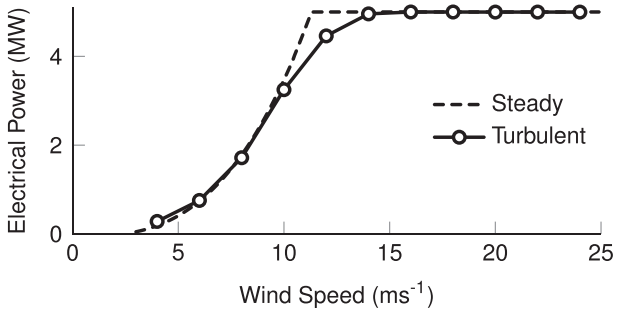

(a) NREL 5 MW

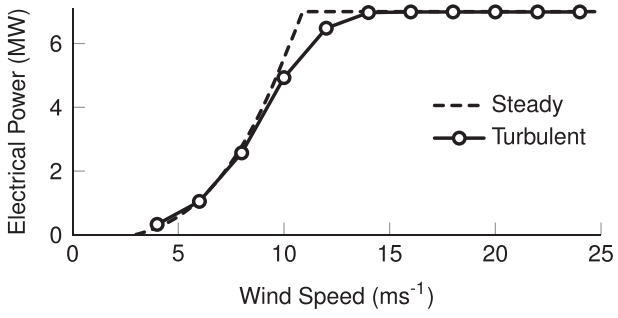

(b) DNV GL 7 MW

Fig. 17. Steady and turbulent power curves.

loss in AEY. It is this dependency of performance and load alleviation, and ultimately CoE, on coupling that requires full exploration.

As a rough estimate of power quality and smoothing effects, the standard deviation σ of electrical power from turbulent simulations is considered. Standard deviation of the electrical power signal represents the average distance from the mean value, therefore, a decrease in σ can be considered a smoothing of the power signal and vice-versa. Such smoothing can have benefits for the grid and electrical components. Percentage differences in standard deviation relative to the baseline are shown for both adaptive blades in Fig. 18.

Both blades display greatest differences in power smoothing in the above-rated regions, however, with opposing trends. The NREL 5 MW displays significant decreases in σ in the above-rated region, a likely benefit of the adaptive behaviour, whilst the 7 MW displays increases. The smoothness of the power signal is reflective of how the WT is dynamically interacting with the turbulence of the wind, with the control regimes playing a key role. In the below-rated region, only the adaptive behaviour alters sectional angles of attack, whereas above-rated, both active and passive control are varying sectional angles of attack in what could either be a synergistic or a detrimental manner, depending on the tuning of the controller. As already stated, the dynamic controller for the 7 MW is a more advanced design than the NREL, and it is likely that differences in power smoothness are attributable to these differences in controller design.

5.2.2. Fatigue analysis

As a further reflection of the adaptive blade's load alleviation capabilities, comparisons in fatigue loading are now made. Fatigue loads in all relevant parts of the WT system are assessed in terms of DEL, where the rainfall cycle counting algorithm [35] is used with a series of load histories. DEL is a constant oscillating load at fixed frequency that, over the WT lifetime, would cause an equal amount of damage to the actual time-varying loads. Load histories are obtained from DLC 1.2 and DLC 6.4 simulations, representing loads during power production and in situations below and above rated. Contributions from each simulation are assumed to be Weibull distributed. The WT lifetime and the number of load cycles are assumed to be 20 years and 10^7, respectively.

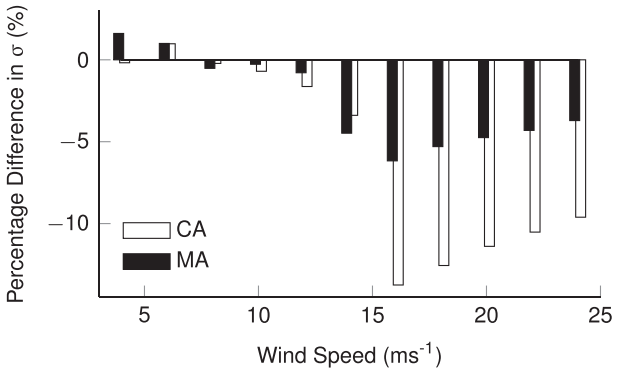

(a) NREL 5 MW

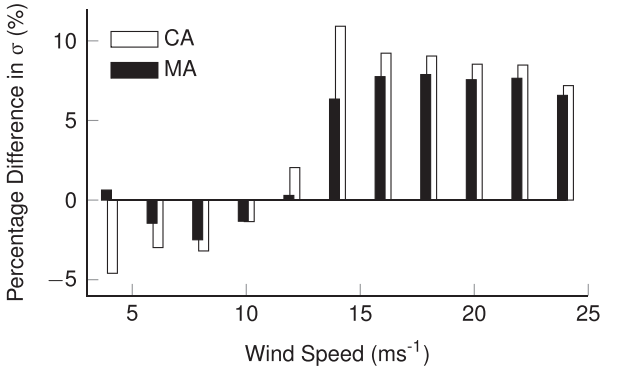

(b) DNV GL 7 MW

Fig. 18. Changes in standard deviation of electrical power.

Results are displayed in Tables 13 and 14, in terms of percentage difference between the adaptive and baseline designs. An increase in blade edgewise root moments (M_x) occurs for all adaptive designs, primarily due to the increases in blade mass as discussed previously. However, whilst the NREL CA blade mass decreases it still displays an increase in edgewise DEL, which is unexpected as all other percentage changes in edgewise DEL correspond, almost exactly, with the respective changes in blade first moment of mass. Similarly to the gust analysis, blade flapwise root moments (M_y) reduce for adaptive blades due to the nose-down twist behaviour. In both cases, the CA causes a greater reduction in flapwise DEL, where reasons for this have been discussed in the gust analysis section. Relatively significant increases in blade torsional root moment (M_z) are shown for both designs, particularly for the CA. For the MA, this behaviour could be due to the extra torsional flexibility, whereas the CA also has this effect in combination with the fact that all aerodynamic loading is offset from the straight pitch axis, due to sweep. It is noted that the magnitude of torsional moment DELs is smaller than bending moment DELs so is not as influential on the overall fatigue damage in the blade; however, they can have a significant effect on the sizing of pitch system components. Therefore, the effects of increasing torsional DELs remain important considerations for aeroelastically tailored blades. Furthermore, it is noted that the detrimental effects of offset aerodynamic loading due to sweep could be partially mitigated by optimisation of the sweep curvature, leading to a blade that sweeps forward near the root and then rearward towards the tip.

Tables 13 and 14 further show that, when compared to their respective baseline values, tower root rolling moments (M_x) decrease for the 5 MW designs, yet increase for the 7 MW designs. This seemingly contradictory result could be explained by considering the combined effects of dynamic controllers and the changes in blade mass due to tailoring (see Table 4). It appears that the range of mass increase (i.e. 7.36% – 9.23%) for the 7 MW blade dominates the increased contribution to tower rolling moment. Whilst in the NREL blade the mass change is smaller (i.e. −2.49% – 2.24%) allowing the effects of the dynamic controllers to drive down changes in tower rolling moment. This situation could be further exacerbated by different control strategies between the two blades. Both the tower root nodding moment (M_y) and the yaw bearing F_x arise as a consequence of the overall thrust force felt by the rotor. Decreases are observed for both WTs, which are notably larger for the CA design. This load reduction is associated with the effects of the blade flapwise load alleviation as well as to changes in rotor mass. Tower yaw moments (M_z) decrease in all cases, particularly for the CA designs, once again due to the effect of the flapwise load alleviation capability. Lastly, the stationary hub moment M_x provides a good indicator of fatigue loading in the shaft and drivetrain. Whilst reductions occur for both MA blades, the MA designs show contradictory results where the increase for the NREL CA design could be due to increased resonance of an edgewise mode.

5.2.3. Pitch system considerations

We now consider the effect of the adaptive blades on the pitch

Table 13
Percentage differences in DELs, relative to the baseline NREL 5 MW.

DEL		MA (%)	CA (%)
Blade Root	M_x	8.8	6.2
	M_y	−5.8	−9.0
	M_z	22.8	56.0
Tower Root	M_x	−3.0	−4.0
	M_y	−3.5	−6.7
	M_z	−11.1	−21.1
Yaw Bearing	F_x	−5.7	−8.8
Stationary Hub	M_x	−3.0	4.6

system and the subsequent consequences on the respective components. Firstly, in a similar fashion to Botasso et al. [11], actuator duty cycle (ADC) is calculated for each design as a measure of actuator usage. Pitch rate histories are obtained from DLC 1.2 simulations. The expressions used for calculating ADC are

$$\mathrm{ADC}(V_k) = \frac{1}{T}\int_0^T \frac{\dot{\beta}(t, V_k)}{\dot{\beta}_{\max}}\, dt, \tag{2}$$

and

$$\mathrm{ADC} = \sum_k F_{V_k}\mathrm{ADC}(V_k), \tag{3}$$

where $\dot{\beta}$ indicates pitch rate as a function of time t, obtained from each simulation of mean wind speed V_k, where k indicates the k^{th} simulation at that wind speed. The term $\dot{\beta}_{\max}$ is the maximum allowable pitch rate, T is the total time for each simulation and F_{V_k} is the Weibull distributed probability of a simulation with that mean wind speed occurring. The percentage changes in ADC, relative to the baseline, are shown in Table 15. Reductions for all adaptive designs are observed, with greater reductions for the CA designs. However, due to the controller not being re-tuned for the adaptive designs, it is not clear how these values could change for a re-tuned, or even redesigned, controller.

Whilst ADC gives a good measure of pitch actuator usage and therefore wear and fatigue damage for some components, it gives no reflection of the load levels in the system. From the fatigue results, relatively significant increases in torsional DEL at the blade root are shown indicating that the adaptive designs could generate greater loads through the pitch system. Considerations from this result include: (i) the effect on power requirements for pitch actuation and (ii) the varying magnitude of the loads in the pitch bearing across its usage.

An average power estimate has been calculated using

Table 14
Percentage differences in DELs, relative to the baseline DNV GL 7 MW.

DEL		MA (%)	CA (%)
Blade Root	M_x	14.0	12.0
	M_y	−6.1	−9.5
	M_z	19.2	37.1
Tower Root	M_x	10.7	6.9
	M_y	−2.1	−3.8
	M_z	−3.2	−9.9
Yaw Bearing	F_x	−2.0	−3.9
Stationary Hub	M_x	−0.9	−0.7

Table 15
Percentage differences in ADC, relative to the baseline.

ADC	MA (%)	CA (%)
NREL 5 MW	−2.25	−6.30
DNV GL 7 MW	−2.57	−3.73

$$\mathrm{Power}(V_k) = \frac{1}{T}\int_0^T \tau\dot{\beta}\, dt, \tag{4}$$

and

$$\mathrm{Power} = \sum_k F_{V_k}\mathrm{Power}(V_k), \tag{5}$$

where τ is pitch actuator torque and $\dot{\beta}$ is pitch rate. As for ADC calculations, the average power usage for each simulation is weighted according to the Weibull distribution of wind speeds. Percentage differences in this average power value, relative to the baseline, are shown in Table 16. Large increases occur for the NREL 5 MW blades whilst small decreases are shown for the 7 MW blades. With the decreases in ADC already observed, this increase in power for the NREL could be solely attributed to the large increases in torsional loading, as observed in the fatigue loads. However, it is interesting that increases have not been shown for the 7 MW blade as there are also increases in torsional DEL, albeit not as large. This difference could be a result of the more advanced controller design, indicating that, whilst swept blades may significantly increase the torsional loads at the blade root, the controller could still alleviate some of the negative effects on power requirements.

5.3. Flutter stability

A flutter analysis is undertaken to show the effects of aeroelastic tailoring on stability margins. The reduction in torsional stiffness and introduction of BTC affect flutter margins, due to the unstable interaction between bending and twisting deformations. Previous work shows flutter to be an increasing concern for larger, more flexible blades [9,10].

To assess stability, an idling simulation is run with a slow ramp up in wind speed. In this simulation, the rotor is not connected to the drivetrain or generator and the pitch angle is fixed at 0 deg, allowing the rotor to rotate freely. The wind speed ramps from 3 ms^{-1} to 20 ms^{-1} over 2000 s so as to avoid increases in rotor speed influencing the point at which instability occurs. The rotor can reach very high tip speeds and thus limits on the applicability of the aerodynamic models are reached due to compressibility effects which are not accounted for. However, this analysis gives a first estimate of safety margins in allowable rotational speeds.

Fig. 19 displays the tip rotation for the 7 MW baseline blade as a function of rotor speed. The occurrence of a flutter instability is shown at the point where the tip rotation grows exponentially and undergoes divergent oscillations, it is noted that only the figure for the 7 MW baseline blade is shown as all other blades show similar

Table 16
Percentage differences in average pitch system power requirements, relative to the baseline.

Pitch Average Power Usage	MA (%)	CA (%)
NREL 5 MW	33.74	108.11
DNV GL 7 MW	−1.56	−8.08

features. Table 17 shows the rotor speeds at which the various blade designs become unstable. It can be seen that the adaptive designs increase the rotor speed at which instability occurs for the NREL blade, whilst entail decreases for the 7 MW blade. In both cases, the CA configuration has a marginally greater stability margin than the MA. It is interesting that the adaptive NREL blades display greater stability margins than the baseline, as one might expect that the introduction of extra torsional flexibility would be detrimental for aeroelastic stability. However, it was found that the results from these analyses were particularly sensitive to blade properties such as polar moment of inertia and shear centre - for which there is some uncertainty in the available literature for the NREL blade. Therefore, it is recommended that caution be taken when interpreting stability results for this blade. In contrast to the findings here, Larwood et al. [9] find that the NREL baseline blade is closer to the flutter boundary, and with geometric BTC, the blade experiences flutter instability at high wind speeds within its operational range.

It is noted that all flutter speeds for the blades presented here are sufficiently large compared to rated rotational speed that this instability would not affect normal operation. Such an instability may only be a cause for concern in fault scenarios where brakes and pitch actuator have stopped working.

6. Conclusions

A comparison of aeroelastically tailored blades has been made, with a focus on energy yield and load alleviation. Overall three overarching conclusions are drawn. First, we confirm results in previous work (e.g. Refs. [11,14–16]) that blade mass increases due to BTC (which can be up to 10% as per Table 4), because the use of more compliant off-axis plies necessitates more material to match the stiffness requirements of the baseline blades. Second, BTC redistributes loads more favourably along the blade and into the tower showing up to 9% reduction in flapwise blade root bending moment and up to 7% in tower root nodding moment (as seen in Tables 13 and 14). Third, there is scope for negligible reductions and potential increases in energy yield for BTC blades analysed in steady simulations.

We expand on these points and present additional conclusions as follows:

- Two adaptive blade configurations are presented, one with material coupling (MA) and the other with combined material and geometric coupling (CA), with the aim of matching baseline stiffnesses, distribution of mass and specific twist deflections. In this way, we near-negligibly impact the global stiffness and dynamic characteristics of the blade and so provide an appropriate comparison with the baseline designs. As a consequence, increases in blade mass are observed, due to the use of more compliant off-axis plies and hence the requirement for more material. However, adaptive designs generally offer potential for reducing blade mass due to the consequent decrease in loads and thus required stiffness.
- Load alleviation is observed from a fatigue analysis for both adaptive blades, with reductions in flapwise blade root (up to 9%), tower root (up to 7%) and drivetrain (up to 9%) DELs as seen in Tables 13 and 14. The CA design is marginally more load alleviating. However, edgewise and torsional blade DELs increase for both blades, with torsional DELs being significantly greater for the CA design. Increases in edgewise DELs are primarily due to the increases in blade mass. However, the inherent BTC also better aligns the aerodynamic loads to the rotor plane, hence increasing the overall rotor torque, whilst redistributing the structural loads more favourably by inducing larger, yet benign, torsional and edgewise stresses. It is assumed that with appropriate re-tuning of the controller, greater load alleviation could be observed.
- Some gains in steady AEY are achieved by the CA blade, whilst the MA blade sees losses. This is an important outcome as twist optimisation studies, as per [14], display negligible potential for such gains. These gains are possibly due to the near-rated region where generator maximum allowable speed is reached slightly before rated wind speed, thus fixing rotor speed and leaving TSR slightly sub-optimal. However, it is recommended that further work be undertaken into understanding precisely where such gains are made. AEY results, averaged from 10-minute turbulent simulations, offer less obvious trends - both adaptive NREL blades show increases on the baseline (0.6%) whilst the 7 MW blades show decreases (−0.5%). The exact source of this disparity in AEY is unclear due to the dynamic WT being such a highly coupled system, however, possible influences include: issues with tuning and design of the dynamic controllers, the particular set of turbulent wind files considered being randomly generated and thus only one of many, and the fact that the blade is designed using steady analysis tools. Future work aims to provide aeroelastically tailored blade designs using optimisation and dynamic tools.
- In a gust scenario, smoothing of electrical power and rotational speed is observed for both adaptive blades. Additionally, flapwise load alleviation and reduced pitch angle and rate are achieved, with the CA performing marginally better than the MA. See Figs. 13–15.
- Reductions in ADC are achieved for the pitch control system (up to 6%, see Table 15). Whilst being a good indicator of load fluctuation, ADC gives no indication of loads. A better indicator is average pitch actuator power usage, where reductions of up to

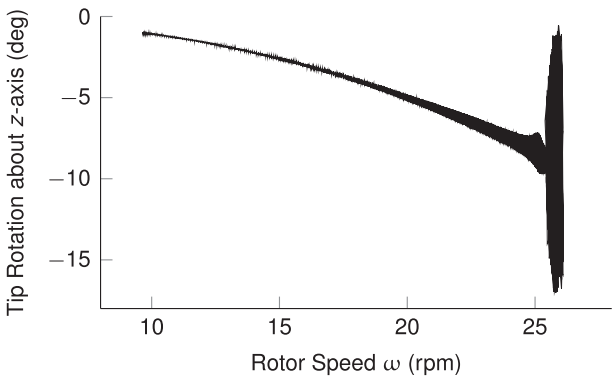

Fig. 19. Stability analysis for the 7 MW baseline - Blade tip z rotation plotted against rotor speed.

Table 17
Flutter speeds for the respective WTs.

(a) NREL 5 MW	
Blade	Flutter Speed (rpm)
B	20.2
MA	21.8
CA	22.8
(b) DNV GL 7 MW	
Blade	Flutter Speed (rpm)
B	25.5
MA	17.5
CA	18.5

8% for the 7 MW adaptive blades and significant increases for the 5 MW adaptive blades are found (see Table 16).

- Optimising blade static-twist offers AEY increases for blades with BTC (see Tables 6 and 7). As the tailoring modifies the torsional coupling, and thus the twist deflection under loading, static-twist must be readjusted to maintain optimal twist angles - with respect to maximising AEY. A similar effect could be obtained by, instead, optimising the set pitch angle β^* (as seen in Ref. [11]) or torque control law (see Section 4.3). Whilst these options have the advantage of not altering blade structural dynamics, they do not offer the same capacity for AEY increase as modifying static-twist. In contrast, Stäblein et al. [31] recover AEY by matching angle of attack distribution of the baseline, at a specific design wind speed. It would be interesting to provide a comparison between the methods presented herein and the work in Ref. [31].
- Increases in flutter stability margin, compared to the baseline, are observed for the adaptive NREL blades, whilst decreases are seen for the 7 MW blades. The CA blades shows marginally greater stability margin than the MA blades. However, the flutter speeds remain well above rated rotor speed so are not dangerous for normal operation. The point at which instability occurs is found to be particularly sensitive to blade properties such as shear centre and polar moment of inertia, therefore, it is necessary that future stability estimations be undertaken with accurate blade properties which, in turn, requires accurate tools for predicting such properties.
- With respect to the initial aim of providing a thorough comparison between the MA and the CA design, the firm conclusion is that the CA achieves a similar level of load alleviation to that of the MA whilst displaying superior steady energy yield. As for which design is most load alleviating, currently neither has been shown to be clearly better than the other. A full exploration of the structural design space is required to ascertain more reliable conclusions. Additionally, as for whether steady power gains can be realised in realistic turbulent simulations, it is necessary to re-tune the dynamic controller for each design. It is also recommended that future comparisons be made for a BTC distribution that is optimised with respect to AEY, loading, or ultimately CoE; rather than for the blades with predefined distributions of coupling used here.
- Whilst the tools used here (PreComp and Bladed) allow the intended coupling effects to be observed, there are limitations with the assumptions used in PreComp including thin-walls, free warping and constant shear flow. To help mitigate uncertainties in analysis of blade cross-sectional properties, future work aims to provide more accurate tools appropriate for analysing blades with complex couplings.

Many effects of adaptive blade design have been considered here, however, the ultimate goal in WT design is reducing CoE. Therefore, this poses the question of what is the optimal adaptive blade, or even system, design with respect to minimising CoE. A well optimised adaptive design may provide power gains and reductions in fatigue and extreme loads. However, new opportunities in design become possible, including increasing blade length for more power or reducing blade mass for lower material costs, whilst possibly retrofitting existing tower and drivetrain infrastructure. The introduction of new design choices then requires a multi-disciplinary optimisation process to find the optimal blade design. Additionally, effects on the pitch system, drivetrain loads, tower loads, manufacturability, modal dynamics, power smoothing and controller design are all important factors. Therefore, it is recommended that multi-disciplinary optimisations with respect to CoE, along the lines of that presented by Vesel et al. [36], are carried out to understand the overall effects of broader design choices.

Data statement

All numerical models and underlying data to reproduce the results and support the conclusions within this paper are available for download from the Research Data Repository of the University of Bristol, https://data.bris.ac.uk/data, at https://doi.org/10.5523/bris.3vvhuzre8xg7i2w1ozs16vd27h.

Acknowledgements

The authors would like to acknowledge the support of the EPSRC under its SUPERGEN Wind Challenge 2015 Grant, EP/N006127/1.

References

[1] F.L. Ponta, A.D. Otero, A. Rajan, L.I. Lago, The adaptive-blade concept in wind-power applications, Energy Sustain. Dev. 22 (2014) 3–12, http://dx.doi.org/10.1016/j.esd.2014.04.004.
[2] X. Lachenal, S. Daynes, P.M. Weaver, Review of morphing concepts and materials for wind turbine blade applications, Wind Energy 16 (2) (2013) 283–307, http://dx.doi.org/10.1002/we.531.
[3] S. Guo, D. Li, Y. Liu, Multi-objective optimization of a composite wing subject to strength and aeroelastic constraints, Proc. Institution Mech. Eng. Part G J. Aerosp. Eng. 226 (9) (2011) 1095–1106, http://dx.doi.org/10.1177/0954410011417789.
[4] D. W. Lobitz, P. S. Veers, P. G. Migliore, Enhanced performance of hawts using adaptive blades, in: Proceedings of the Wind 1996 ASME Wind Energy Symposium. Houston, TX, 1996.
[5] K. Hayat, S.K. Ha, Load mitigation of wind turbine blade by aeroelastic tailoring via unbalanced laminates composites, Compos. Struct. 128 (2015) 122–133, http://dx.doi.org/10.1016/j.compstruct.2015.03.042.
[6] M.T. Herath, A.K. Lee, B. Gangadhara Prusty, Design of shape-adaptive wind turbine blades using differential stiffness bend-twist coupling, Ocean. Eng. 95 (2015) 157–165, http://dx.doi.org/10.1016/j.oceaneng.2014.12.010.
[7] Knight & Carver Wind Group, Sweep-twist Adaptive Rotor Blade: Final Project Report, Tech. Rep. SAND2009-8037, Sandia National Laboratories, Albuquerque, NM, 2010.
[8] C. Findlay, Blades with a twist, in: Living Energy, July 2013 no. 8, Siemens.
[9] S. Larwood, C.P. van Dam, D. Schow, Design studies of swept wind turbine blades, Renew. Energy 71 (2014) 563–571, http://dx.doi.org/10.1016/j.renene.2014.05.050.
[10] D.W. Lobitz, Aeroelastic stability predictions for a MW-sized blade, Wind Energy 7 (3) (2004) 211–224, http://dx.doi.org/10.1002/we.120.
[11] C.L. Bottasso, F. Campagnolo, A. Croce, C. Tibaldi, Optimization based study of bend-twist coupled rotor blades for passive and integrated passive/active load alleviation, Wind Energy 16 (8) (2013) 1149–1166, http://dx.doi.org/10.1002/we.1543.
[12] M. O. Gözcü, M. N. Olgun, A. Kayran, Investigation of the effect of off-axis spar cap plies on damage equivalent loads in wind turbines with superelement blade definition, J. Phys. Conf. Ser. 524. http://dx.doi.org/10.1088/1742-6596/524/1/012040.
[13] J. Jonkman, S. Butterfield, W. Musial, G. Scott, Definition of a 5 Mw Reference Wind Turbine for Offshore System Development Definition of a 5 Mw Reference Wind Turbine for Offshore System Development, Tech. Rep. NREL/TP-500–38060, National Renewable Energy Laboratory, 2009.
[14] M. Capuzzi, A. Pirrera, P.M. Weaver, A novel adaptive blade concept for large-scale wind turbines. part I: aeroelastic behaviour, Energy 73 (2014) 15–24, http://dx.doi.org/10.1016/j.energy.2014.06.044.
[15] M. Capuzzi, A. Pirrera, P.M. Weaver, A novel adaptive blade concept for large-scale wind turbines. part II: structural design and power performance, Energy 73 (2014) 25–32, http://dx.doi.org/10.1016/j.energy.2014.04.073.
[16] M. Capuzzi, A. Pirrera, P.M. Weaver, Structural design of a novel aeroelastically tailored wind turbine blade, Thin-Walled Struct. 95 (2015) 7–15, http://dx.doi.org/10.1016/j.tws.2015.06.006.
[17] M. Capuzzi, Aeroelastic Tailoring of Wind Turbine Blades for Power Improvement and Load Alleviation, Ph.D. thesis, University of Bristol, 2014.
[18] C. Lindenburg, Aeroelastic Modelling of the LMH64-5 Blade, Tech. rep., DOWEC Research Project, 2002.
[19] IEC 61400-1, Wind Turbines - Part 1: Design Requirements, IEC, 2005.
[20] H. Glauert, An Aerodynamic Theory of the Airscrew, Vol. 786 of Reports and Memoranda, Great Britain Aeronautical Research Committee, H. M. Stationery Office, 1922.
[21] L. Prandtl, O. Tietjens, Applied Hydro and Aeromechanics, Dover Publications, 1957.
[22] D.M. Pitt, D.A. Peters, Theoretical prediction of dynamic inflow derivatives, in: Sixth European Rotorcraft and Powered Lift Aircraft Forum, 1980.

[23] J.G. Leishman, T.S. Beddoes, A semi-empirical model for dynamic stall, J. Am. Helicopter Soc. 34 (3) (1989) 3–17.
[24] S. Øye, Dynamic stall simulated as time lag of separation, in: Proceedings of the 4th IEA Symposium on the aerodynamics of wind turbines, 1991.
[25] P.E. Nikravesh, Computer-aided Analysis of Mechanical Systems, Prentice-Hall, 1988.
[26] DNV GL, Bladed Theory Manual, 2014, http://dx.doi.org/10.1007/s13398-014-0173-7.2.
[27] G.S. Bir, User's Guide to PreComp – Pre-processor for Computing Composite Blade Properties, 2005.
[28] I.M. Daniel, O. Ishai, Engineering Mechanics of Composite Materials, Oxford University Press, 2006.
[29] A. Pirrera, M. Capuzzi, N. Buckney, P. M. Weaver, Optimization of wind turbine blade spars, in: 53rd AIAA/ASME/ASCE/AHS/ASC Structures, Structural Dynamics and Materials Conference, Honolulu, HI, 2012, AIAA 2012-1500. http://dx.doi.org/10.2514/6.2012–1500.
[30] H. Chen, W. Yu, M. Capellaro, A critical assessment of computer tools for calculating composite wind turbine blade properties, Wind Energy 13 (6) (2010) 497–516, http://dx.doi.org/10.1002/we.372.
[31] A.R. Stäblein, C. Tibaldi, M.H. Hansen, Using pretwist to reduce power loss of bend-twist coupled blades, in: 34th Wind Energy Symposium, AIAA SciTech Forum, San Diego, CA, 2016, http://dx.doi.org/10.2514/6.2016-1010. AIAA 2016-1010.
[32] E. Alpman, Effect of selection of design parameters on the optimization of a horizontal axis wind turbine via genetic algorithm, J. Phys. Conf. Ser. 524 (2014) 012044, http://dx.doi.org/10.1088/1742-6596/524/1/012044.
[33] L. Diaz-Guerra, F.D. Adegas, J. Stoustrup, M. Monros, Adaptive control algorithm for improving power capture of wind turbines in turbulent winds, in: American Control Conference (ACC), vol. 2012, 2012, pp. 5807–5812, http://dx.doi.org/10.1109/ACC.2012.6315452.
[34] L.I. Lago, F.L. Ponta, A.D. Otero, Analysis of alternative adaptive geometrical configurations for the nrel-5 mw wind turbine blade, Renew. Energy 59 (2013) 13–22, http://dx.doi.org/10.1016/j.renene.2013.03.007.
[35] S. Downing, D. Socie, Simple rainflow counting algorithms, Int. J. Fatigue 4 (1) (1982) 31–40, http://dx.doi.org/10.1016/0142-1123(82)90018-4.
[36] R.W. Vesel, J.J. McNamara, Performance enhancement and load reduction of a 5 mw wind turbine blade, Renew. Energy 66 (2014) 391–401, http://dx.doi.org/10.1016/j.renene.2013.12.019.